RSC Advances

ROYAL SOCIETY OF CHEMISTRY

www.rsc.org/advances

Journal Name

RSCPublishing

PAPER

Pd modified kaolinite nanocomposite as hydrogenation catalyst

Cite this: DOI: 10.1039/x0xx00000x

Xiaoyu Li [a,b], Aidong Tang [c,*]

Received 00th January 2012,
Accepted 00th January 2012

DOI: 10.1039/x0xx00000x

www.rsc.org/

A preparation strategy for palladium (Pd) nanoparticles anchored on the surface of kaolinite nanorods to form Pd/kaolinite nanocomposite and the highly efficient catalytic hydrogenation performance has been presented in this paper. Natural kaolinite nanorod served as a mild and outstanding stabilizer for supporting Pd nanoparticles. The results indicated that well-dispersed Pd nanoparticles successfully anchored on kaolinite nanorods via self-assembly method. Natural rod-like kaolinite possessing hydroxyl groups on its surface serves as an ideal nanoscale support for assembly and integration with Pd particles. Thus, it was revealed that kaolinite nanorods not only interacted favorably with the Pd species, but also acted as a support that suppressed the aggregation and precipitation of the Pd nanoparticles. The nanocatalyst was found to be effective for the catalytic hydrogenation of styrene to ethylbenzene. The process of catalytic hydrogenation was further depicted.

1. Introduction

Nanostructured noble metallic particles are attracting tremendous attention for advanced versatile applications such as heterogeneous catalysts[1], hydrogen storage[2], gas sensors[3] and photovoltaic devices[4], or fuel cells[5]. Noble metal-based catalysts are preferred for deep hydrogenation since they can work at lower temperatures. In addition, Pd-based catalysts are able to maintain high activities of hydrogenation compared to transition metal catalysts. At present, matrices used for supporting Pd nanoparticles are polystyrene spheres[6], carbon materials[7], oxide[8, 9], mesoporous materials[10, 11], silica spheres[12], natural and artificial polymers[13], and clay minerals[14] (such as palygorskite[15],montomorillonite[16-18], halloysite[19]). Although the preparation of these samples was successful, majority of the approaches involve complicated surface modifications using organic surfactants or polymeric ligands to inhibit particles agglomeration. However, the addition of organic dispersants could have negative consequences on various applications which were unwanted organic residues. Meanwhile, selection of the matrix for composite materials depends on the material's application[20-22]. Therefore, a facile route devoid of organic modification agents to synthesize nanosized Pd-based catalysts has become highly desirable.

[a] *Centre for Mineral Materials, School of Minerals Processing and Bioengineering, Central South University, Changsha 410083, China*

[b] *Key Laboratory for Mineral Materials and Application of Hunan Province, Central South University, Changsha 410083, China*

[c] *School of Chemistry and Chemical Engineering, Central South University, Central South University, Changsha 410083, China*

[*] *Corresponding author, email: adtang@csu.edu.cn, Tel.: +86-731-88879616, Fax: +86-731-88879616.*

It is well known that surface of clay minerals possess plentiful hydroxyl groups, which usually act as protective groups to prevent nanoparticles from coagulating by binding to the particle surface and enhance their stability[23, 24, 25]. Kaolinite ($Al_2Si_2O_5(OH)_4$) is a 1:1-type clay type clay mineral composed of stacked layers of SiO_4 tetrahedral sheets and $AlO_2(OH)_4$ octahedral sheets and naturally possesses a nanorod-like morphology. It is a suitable catalytic support provided with the strong ability to stabilize and disperse noble metal nanoparticles. Recently, kaolinite nanorods have gained a great deal of interest due to their multi-faceted applications in optical devices[26], catalyst[27], and thermal energy storage materials[28,29,30]. On the other hand, immobilization of catalytically active noble metals on the heterogeneous support has drawn significant interest. Therefore, employing kaolinite nanorods as a catalyst support, which possess many hydroxyl groups on its surface would be highly promising because of their good surface property and ease of functionalization. Pd/kaolinite nanocomposites described herein showed high catalytic hydrogenation activity.

In this work, we have successfully synthesized Pd/kaolinite nanocomposites via anchoring Pd nanoparticles on the surface of kaolinite nanorods under ambitious conditions. Furthermore, we chose the catalytic hydrogenation of styrene in the liquid phase as the model reaction to evaluate the catalytic performance of catalysts. Moreover, atomic-level hydrogenation process for room-temperature hydrogenation of styrene was clarified.

2. Experimental

2.1 Materials preparation

Kaolin (kaolinite>95%) used in this study was obtained from Fujian, China, possessed the natural nanorod-like morphology. Other reagents were analytical grade without further purification. In a

typical synthesis, a dispersion of kaolinite (0.5, 1.0 and 1.5 g) in 10 mL deionized water was homogenized in an ultrasonic bath for 1 h at room temperature, and followed by the addition of aged Na_2PdCl_4 solution (500 μL, 5 wt%) to each clay solution with continuous stirring for 2 h. The mixed solutions containing clay and Pd species were maintained in the dark under static conditions at room temperature. The formation of Pd nanoparticles was indicated by a color change in the reaction solution from brown to black within 24 h of mixing. After collection by centrifugation, the final products were washed with distilled water repeatedly and dried at 60 ℃ in a vacuum oven. The nominal Pd loading amount of Pd/kaolinite composites were 3.0%, 1.5% and 1.0%, respectively.

2.2 Characterization

Powder X-ray diffraction (XRD) measurements of the samples were recorded on a DX-2700 X-ray diffractometer using Cu Kα radiation (λ=0.15406 nm) at a scanning rate of 0.02 deg/s with a voltage of 40 kV and 40 mA. Scanning electron microscopy (SEM) was performed with a JEOL JSM-6360LV scanning electron microanalyzer with an accelerating voltage of 5 kV. Transmission electron microscopy (TEM) studies were performed using a JEOL JEM-2100F operating at 200 kV and equipped with EDS capabilities. The morphology of Pd/kaolinite was observed with a high-resolution transmission electron microscopy (HRTEM, JEOL JEM-3010). The samples for TEM analysis were dispersed in ethanol by ultrasonication and a drop of each solution was deposited on a Cu grid coated by a holed carbon film and subsequently dried in air. Fourier transform infrared (FTIR) spectra of the samples over the range of 4000~400 cm^{-1} were recorded on a Nicolet Nexus 670 FTIR spectrophotometer using KBr pellets. X-ray photoelectron spectroscopy (XPS) measurements were performed on a Thermo Fisher Scientific K-Alpha 1063 equipped with a hemispherical electron analyzer and an Al Kα X-ray radiation source (1486.6 eV), a voltage of 15 kV, and an emission current of 10 mA. To compensate for surface charge effects, the XPS results were calibrated using the C 1s hydrocarbon peak at 284.6 eV. The N_2 adsorption isotherms were recorded at 77 K and analyzed using an ASAP 2020 surface area analyzer (Micromeritics Co. Ltd.). The catalytic hydrogenation of styrene reaction was monitored by gas chromatographic (SHIMADZU 2010, column RTX-5 with inner diameter 0.25 mm, film depth 0.25 μm and length 30 m) analysis of the solution withdrawn from the reactor for a given time.

2.3 Catalytic activity

The catalytic hydrogenation of styrene to ethylbenzene was carried out in a 150 mL glass batch reactor equipped with a magnetic stirrer at 25 ℃ at atmospheric pressure. Moreover, an additional stability test was performed under the same conditions. For each experiment, 100 mg sample was firstly suspended in 100 mL ethanol together with 0.1 mL *n*-decane (used as the internal standard) and pretreated in H_2 flow (40 mL/min) at 25 ℃ for 1 h. Then 1 mL styrene was added into the solution in H_2 flow under stirring at room temperature and atmosphere pressure. 1 mL solution was withdrawn and filtered for gas chromatographic test for a given time. After the catalytic test, the catalyst solution was filtered and the catalyst precipitate was re-suspended in ethanol for the next run. The styrene conversion efficiency was calculated as: styrene conversion efficiency (%) = $(M_0 - M_t)/M_0 \times 100\%$, where M_0 is the the initial amount of styrene in the solution, and M_t is amount of styrene of the reation solution at reaction time *t*. k was the reaction rate for each catalyst in the styrene hydrogenation reaction, which was calculated from the slope of the straight line to show the activity of the catalyst in terms of 10^{-3}/min.

3. Results and discussion

Fig. 1a showed the XRD patterns of the as-synthesized Pd/kaolinite

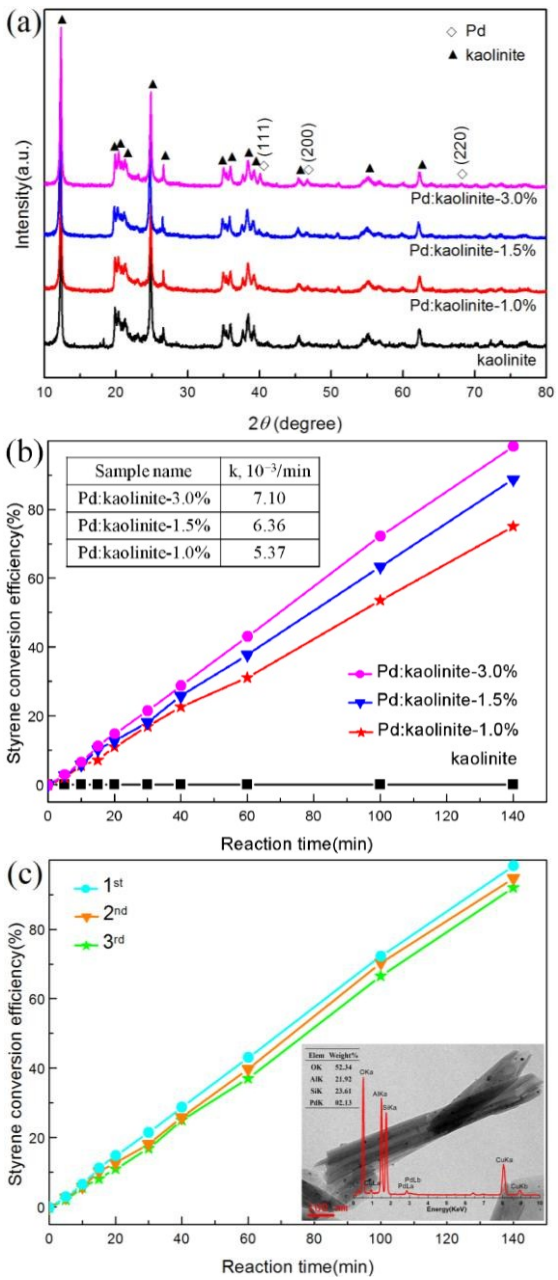

Fig. 1 (a) XRD patterns and (b) styrene hydrogenation reaction curves of kaolinite and Pd/kaolinite with different Pd:kaolinite mass ratios (inset table gave the reaction rate of different catalysts). (c) The stability of Pd:kaolinite-3.0% for styrene hydrogenation reaction (inset was TEM image and EDS spectra of Pd:kaolinite-3.0% after repeating the hydrogenation reaction for 3 cycles).

composite obtained with different Pd:kaolinite mass ratios. The reflections at 2θ of about 40.1 °, 46.7 ° and 68.1 ° all corresponded to the crystal planes of the (111), (200) and (220) of face-centered cubic (fcc) palladium (JCPDS standard card No.65-2867, space group: *Fm3m*)[31], while additional peaks corresponded well to kaolinite[32] and no other crystalline impurities could be detected. Obviously, the structure of kaolinite kept maintained after the introduction of Pd nanoparticles. The broad distribution and low intensities of the above-mentioned peaks were due to the low incorporation of Pd. In addition, the intensity of the Pd reflections became more apparent in the samples synthesized from a higher Pd: kaolinite mass ratio. Catalytic activity data of the catalysts for styrene hydrogenation were compared in Fig. 1b. It was obvious that little change existed for the kaolinite nanorods, which indicated that the kaolinite itself has no catalytic activity. However, the kaolinite possesses a natural nanorod-like morphology and plentiful hydroxyl groups on its surface to avoid Pd nanoparticles aggregation and movement, thus leading to a higher catalytic efficiency. Meanwhile, kaolinite has good adsorption performance and the specific surface area measure in the experiment was 26.6 m^2/g, which was beneficial for the Pd nanoparticles immobilization on the kaolinite surface. According to the reference[33], styrene hydrogenation intrinsic kinetics coincides with zeroth-order reaction law, therefore, the rate of the conversion of styrene keeps constant in the entire reaction process.

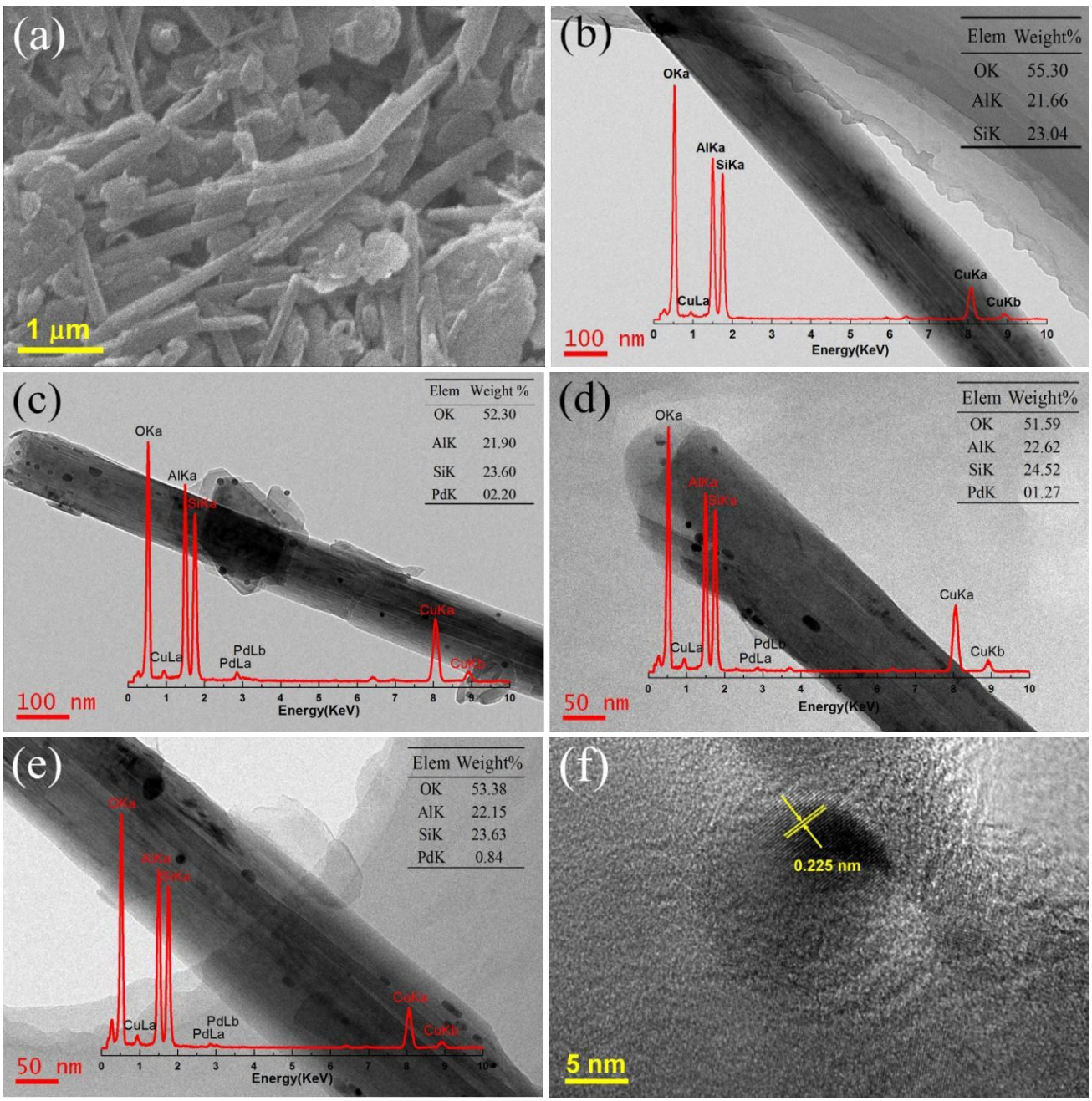

Fig. 2 (a) SEM and (b) TEM images of kaolinite; TEM images of Pd/kaolinite composites: (c) Pd:kaolinite-3.0%, (d) Pd:kaolinite-1.5%, (e) Pd:kaolinite-1.0%, insets in (b-e) were the EDS spectra and corresponding elemental compositions. (f) HRTEM image of Pd:kaolinite-3.0%.

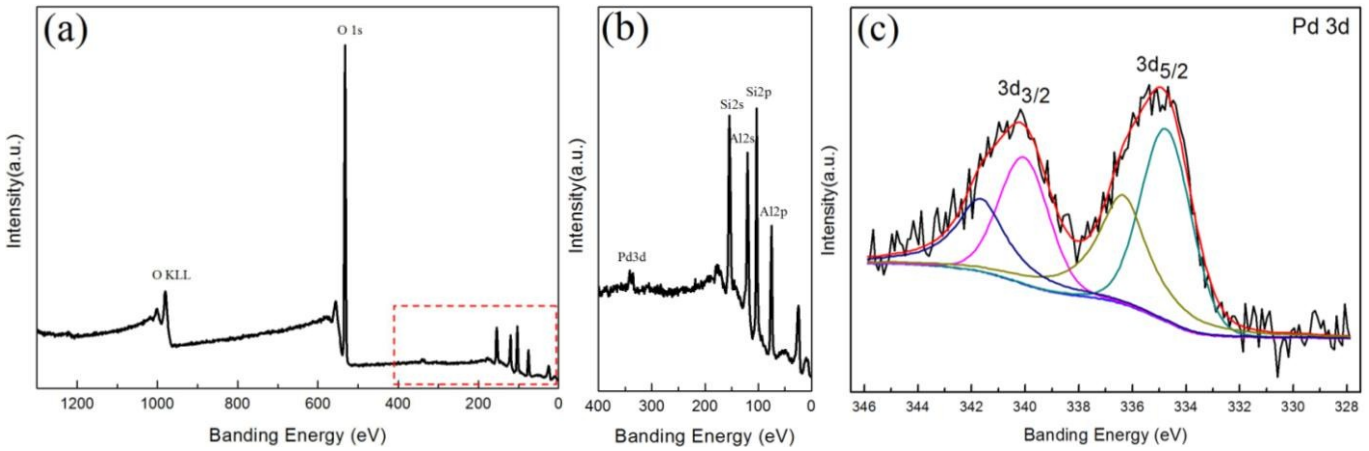

Fig. 3 XPS spectra of Pd:kaolinite-3.0%: (a) survey-scan; (b) magnified part of the corresponding area in (a); (c) Pd 3d spectra.

For Pd/kaolinite composites, the initial reaction rate was calculated from the slope of the straight line to give the activity of the catalyst in terms of 10^{-3}/min and the results were listed in Fig.1b. Comparing with the catalytic efficiency in the references, it was showed that the as-synthesized nanocatalysts were more effective for the catalytic hydrogenation of styrene to ethylbenzene, and the styrene conversion efficiency reached about 75%, 89% and 100% in 140 min for catalysts with the increase of Pd:kaolinite mass ratio, while the styrene conversion efficiency of Pd–Pc complex in the reference was only about 50%[34]. Meanwhile, the as-synthesized samples were achieved under very mild conditions without adding extra polymeric ligands. Michal Sabo et. al.,[35] have reported the palladium loaded on MOF-5 had a high catalytic activity in styrene hydrogenation comparable to that of palladium on activated carbon. The concentration of ethylbenzene after 8 h was 97 wt%. Antje Henschel et. al.,[36] investigated the catalytic activity of Pd/MIL-101 in the hydrogenation reaction, and compared with other catalysts. It was shown that the use of Pd/MIL-101 as a hydrogenation catalyst led to a complete conversion of styrene to ethylbenzene after 7 h. However, other catalysts, under the same reaction conditions, Pd/MOF-5 yielded 80 wt% hydrogenation products after the same reaction time whereas Pd/Norit A afforded ~65 wt% and Pd/C less than 50 wt% ethylbenzene. Meanwhile, the stability of Pd/kaolinite (Pd:kaolinite-3.0%) has been investigated by repeating the hydrogenation reaction for 3 cycles and the TEM image and EDS spectra of Pd:kaolinite-3.0% after repeating the reaction for 3 cycles was showed in Fig. 1c. It was clearly showed that the catalyst was almost stable after circulating cycles and the real Pd loading amount (2.13%) was decreased a little than before (2.2%). The TEM result was consistent with the recycling catalytic results.

Obviously, according to the results mentioned above, some approaches involved complicated polymeric ligands and other experiments conducted under high temperature and pressure. The comparison and analysis indicated that kaolinite was a suitable support for catalytic application. Furthermore, the catalyst with a higher Pd:kaolinite mass ratio exhibited higher styrene catalytic hydrogenation activity.

Typical SEM and TEM images of kaolinite indicated that the kaolinite possessed the natural nanorod-like morphology and smooth surface without contamination with 2~5 μm in length and 0.1~0.3 μm in diameter (Fig. 2a&b). The images of Pd/kaolinite composites clearly indicated that the Pd nanoparticles with particle size of about 8.67 nm (Pd:kaolinite-3.0%, Fig.2c), 9.43 nm (Pd:kaolinite-1.5%, Fig.2d), and 12.71 nm (Pd:kaolinite-1.0%, Fig.2e) were isolated and well-dispersed throughout the kaolinite rod without severe agglomeration via self-assembly. The results indicated that the average size of Pd nanoparticles of Pd/kaolinite composites had decreased trend with increasing Pd loading amount, which was possible because when the Pd:kaolinite mass ratio was lower, the crystal nucleus was relatively less and could grow up into a large size particles. When the Pd:kaolinite mass ratio was larger, there were more crystal nucleus in the solution and the crystal nucleus grew up separately to form more uniform and smaller particles. The typical HRTEM image of Pd:kaolinite-3.0% shown in Fig. 2f depicted clearly visible lattice fringes that evinced the formation of Pd nanoparticles. And the average lattice spacing of 0.225 nm (marked in Fig. 2f) corresponds to the (111) plane of metallic Pd[37]. The corresponding EDS spectra of the surface of as-prepared Pd/kaolinite composites suggested that the presence of Pd, Al, O and Si, which confirmed the existence of Pd nanoparticles on the kaolinite nanorods. With the increase of Pd:kaolinite mass ratios, the real amount of Pd nanoparticles loading was about ~0.84, 1.27 and 2.20 wt%, respectively. The kaolinite nanorods possessing rich surface hydroxyl groups could interact with palladium ions in the solution and avoid Pd nanoparticles aggregation and movement, so leading to a higher catalytic effciency.

XPS analysis was conducted to investigate the surface states and chemical compositions of as-synthesized Pd/kaolinite, as shownin Fig. 3. The measurement further indicated the presence of the interaction between Pd nanoparticles and kaolinite rods. A wide survey scan of XPS spectra was taken in the range 1300~0 eV (Fig. 3a), and the magnified part over the range of 400~0 eV was shown in Fig. 3b. The peaks corresponding to Al, Si, O and Pd were observed, and the Al, Si and O elements were found to derive from the surface of the kaolinite nanorods. No extra peaks corresponding to impurities. Fig. 3c showed the high-resolution fitted XPS spectra of Pd 3d to verify the state of Pd, which indicated that Pd/kaolinite (Pd:kaolinite-3.0%) contained two different Pd surface species. Pd $3d_{5/2}$ and Pd $3d_{3/2}$ peaks observed at about 334.7 and 339.9 eV were ascribed to the metallic Pd only, whereas peaks at approximately

336.4 and 341.7 eV were corresponded to Pd $3d_{5/2}$ and Pd $3d_{3/2}$ peaks of oxidized Pd–O species, respectively[38]. The coexistence of Pd(0) and Pd(II) suggested that the reduction process led to only a partial reduction of Pd(II) to Pd(0) for Pd/kaolinite. After the Pd particles assembling on the kaolinite, the binding energies assigned to Pd(0) ($3d_{5/2}$ = 334.7 eV, $3d_{3/2}$ = 339.9 eV) was lower than those of pure Pd ($3d_{5/2}$ = 335.1 eV, $3d_{3/2}$ = 340.3 eV). The binding energy shifts indicated the presence of the interaction between Pd nanoparticles and kaolinite rods.

The FTIR spectra of kaolinite and Pd/kaolinite were recorded in Fig. 4. The bands at 545, 470 and 429 cm^{-1} were attributed to the vibration of Si–O–Al[39]. The bands at 793, 753 and 690 cm^{-1} were due to the translational vibration of O–Al–OH[40, 41]. The other bands at 3658, 1116, 1033 and 915 cm^{-1} were assigned to inner surface hydroxyl out-of-phase stretching vibration, apical Si–O stretching vibration, skeleton Si–O–Si stretching vibration and the bending vibration of inner Al–OH groups, respectively[39, 41]. Meanwhile, the absorption bands at 3736, 3694 and 3620 cm^{-1} were ascribed to Si–OH stretching vibration, inner-surface hydroxyl stretching vibration for kaolinite sample[41-43]. After loading Pd nanoparticles on the kaolinite nanorods, the peaks were similar to that of kaolinite, except for the peaks at 3620 cm^{-1} and from 1300 to 400 cm^{-1}, which were attributed to inner –OH stretching vibration and some Al–OH groups. As the Pd nanoparticles decorated on the kaolinite nanorods, the bands corresponding to vibrations of inner –OH stretching vibration at 3620 cm^{-1} and Al–OH vibration at 915, 793, 753 and 690 cm^{-1} decreased. Furthermore, according to the reference[44], it was indicated that molecular interactions between the Pd species and hydroxyl groups on the surface of the kaolinite nanorods instigated the anchor of the Pd species. Pd nanoparticles were then generated, and they underwent well-controlled growth while adhering to the kaolinite nanorods. It was reported that silanol moieties on silica-rich substrates could induce the reduction of the Pd species. In the aqueous clay dispersion in the present study, it was feasible that the silanol groups on the surfaces of the kaolinite nanorods induced the relatively mild in situ reduction of the Pd species. In the aqueous solution of Na_2PdCl_4, the $PdCl_4^{2-}$ ions underwent the following solvolysis reactions:

$$PdCl_4^{2-} + H_2O \rightleftarrows PdCl_3(H_2O)^- + Cl^- \quad (1)$$

$$PdCl_3(H_2O)^- + H_2O \rightleftarrows PdCl_2(H_2O)_2 + Cl^- \quad (2)$$

When a known amount of aqueous Na_2PdCl_4 solution was added to the clay dispersion with stirring, the Pd ions interacted with the silanol groups (Si−OH) and form the complex under the preparation conditions. Subsequently, reduction of the Pd species was mildly induced by the silanol groups, and the resulting Pd nanoparticles adhered to the kaolinite.

$$2SiOH + PdCl_2 \rightarrow SiOSi + Pd + 2HCl \quad (3)$$

Based on the above analysis, the experimental process diagram for room-temperature hydrogenation of styrene (Fig. 5) was shown to exhibit the process of catalytic hydrogenation. When hydrogen molecules were absorbed on the surface of Pd nanoparticles, and the surface reaction was performed. As a result, hydrogen molecules were dissociated into hydrogen

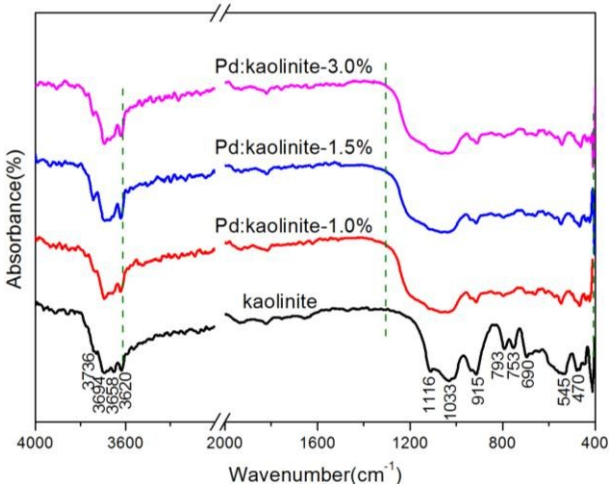

Fig. 4 FTIR spectra of kaolinite and Pd/kaolinite with different Pd:kaolinite mass ratios.

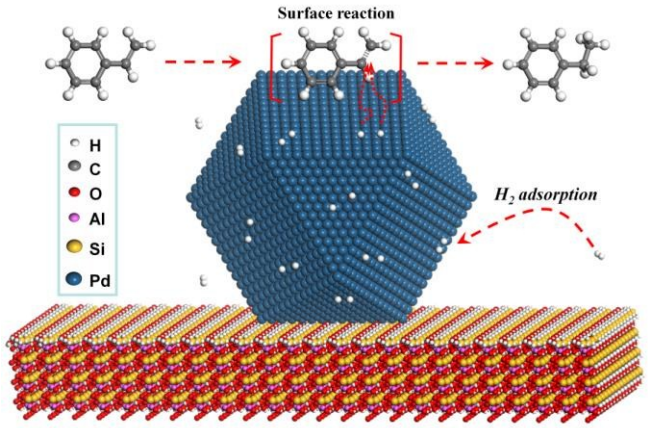

Fig. 5 The schematic diagram for catalytic hydrogenation of styrene at room-temperature.

atoms. H_2 dissociation was a very essential surface reaction on noble metal to hydrogenate the organic molecule[45]. In the process of hydrogenation, styrene adsorbed on the Pd surface was attacked by hydrogen atoms activated by Pd nanoparticles. Finally, styrene was converted to ethylbenzene. It appeared likely that this process was strongly affected by Pd dispersion or the particle size of the Pd nanoparticles. The kaolinite nanorod possessing high length-diameter ratio and rich surface hydroxyl groups is an ideal nanoscale support. Furthermore, it was reported that hydroxyl groups on the surfaces of clay could interact with metal ions in the solution and contribute to the nanopartiles anchored on the clay[44]. When a known amount of kaolinite dispersion was added to the Na_2PdCl_4 solution with stirring, the Pd ions interact with the surface –OH groups and form the complex under the preparation conditions. After in-situ reduction, strong interactions were existed between the surface –OH on kaolinite nanorods and Pd particles, which could avoid Pd nanoparticles aggregation and movement. And it was also identified by FTIR data (Fig. 4), thus leading to a higher catalytic effciency.

4. Conclusions

This paper proposed a facile route to synthesize remarkably functional Pd nanocomposites using kaolinite nanorods without any modifications at room temperature. Palladium nanoparticles were successfully assembled on the surface of kaolinite nanorods to form Pd/kaolinite nanocomposite. Palladium nanoparticles were well-dispersed on the surface of kaolinite nanorods. The kaolinite possessing rich surface hydroxyl groups and high length-diameter ratio make it could avoid Pd nanoparticles aggregation and movement, thus leading to a higher catalytic effciency. It was showed that the catalyst with a higher Pd:kaolinite mass ratio exhibited higher catalytic hydrogenation activity in the liquid phase hydrogenation of styrene to ethylbenzene. Moreover, atomic-level hydrogenation process for room-temperature hydrogenation of styrene was clarified. We believe that the as-synthesized Pd/kaolinite nanocomposites could have interesting potential application in the catalytic fields.

Acknowledgements

This work was supported by the National Natural Science Fundation of China (51374250) and the Hunan Provincial Innovation Foundation for Postgraduate (CX2014B093).

Notes

This manuscript was presented in the form of an abstract at Joint Conference of 5th UK-China and 13th UK Particle Technology Forum, 12-15 July 2015, Leeds, UK

References

1. B. Yoon and C. M. Wai, *J Am Chem Soc*, 2005, **127**, 17174-17175.
2. A. Reyhani, S. Z. Mortazavi, S. Mirershadi, A. Z. Moshfegh, P. Parvin and A. N. Golikand, *J Phys Chem C*, 2011, **115**, 6994-7001.
3. M. Yuasa, T. Kida and K. Shimanoe, *ACS Appl Mater Interfaces*, 2012, **4**, 4231-4236.
4. C.-H. Kim, S.-H. Cha, S. C. Kim, M. Song, J. Lee, W. S. Shin, S.-J. Moon, J. H. Bahng, N. A. Kotov and S.-H. Jin, *ACS Nano*, 2011, **5**, 3319-3325.
5. B. Narayanamoorthy, K. K. R. Datta, M. Eswaramoorthy and S. Balaji, *ACS Appl Mater Interfaces*, 2012, **4**, 3620-3626.
6. H. G. V. G. Pol and A. Gedanken, *Langmuir*, 2005, **21**, 3635-3640.
7. L. Ren, L. Yang, P. Yu, Y. Wang and L. Mao, *ACS Appl Mater Interfaces*, 2013, **5**, 11471-11478.
8. S. K. Mohapatra, N. Kondamudi, S. Banerjee and M. Misra, *Langmuir*, 2008, **24**, 11276-11281.
9. X. Li and H. Yang, *Appl. Clay Sci.*, 2014, **100**, 43-49.
10. K. Okumura, T. Honma, S. Hirayama, T. Sanada and M. Niwa, *J Phys Chem C*, 2008, **112**, 16740-16747.
11. L. Fu, C. Huo, X. He and H. Yang, *RSC Adv.*, 2015, **5**, 20414-20423.
12. Z. Chen, Z.-M. Cui, P. Li, C.-Y. Cao, Y.-L. Hong, Z.-y. Wu and W.-G. Song, *J Phys Chem C*, 2012, **116**, 14986-14991.
13. B. Hu, T. Wu, K. Ding, X. Zhou, T. Jiang and B. Han, *J Phys Chem C*, 2010, **114**, 3396-3400.
14. X. Li, J. Ouyang, Y. Zhou and H. Yang, *Sci. Rep.*, 2015, **5**, 13763.
15. X. He and H. Yang, *J. Mol. Catal. A: Chem.*, 2013, **379**, 219-224.
16. M. Crocker, R. H. M. Herold, J. G. Buglass and P. Companje, *J Catal*, 1993, **141**, 700-712.
17. K. Peng, L. Fu, J. Ouyang and H. Yang, *Adv Funct Mater*, 2016, DOI: 10.1002/adfm.201504942.
18. K. Peng, L. Fu, H. Yang and J. Ouyang, *Sci. Rep.*, 2016, **6**, 19723.
19. Y. Zhang, X. He, J. Ouyang and H. Yang, *Sci. Rep.*, 2013, **3**, 2948.
20. X. He and H. Yang, *Dalton Trans.*, 2015, **44**, 1673-1679.
21. Q. Yang, M. Long, L. Tan, Y. Zhang, J. Ouyang, P. Liu and A. Tang, *ACS Appl Mater Interfaces*, 2015, **7**, 12719-12730.
22. M. Long, L. Tan, H. Liu, Z. He and A. Tang, *Biosens Bioelectron*, 2014, **59**, 243-250.
23. Y. Zhang, A. Tang, H. Yang and J. Ouyang, *Appl. Clay Sci.*, 2016, **119**, 8-17.
24. X. He, Q. Yang, L. Fu and H. Yang, *Funct Mater Lett*, 2015, **8**, 1550056.
25. J. Jin, L. Fu, J. Ouyang and H. Yang, *Sci. Rep.*, 2015, **5**, 12429.
26. E. H. de Faria, E. J. Nassar, K. J. Ciuffi, M. A. Vicente, R. Trujillano, V. Rives and P. S. Calefi, *ACS Appl Mater Interfaces*, 2011, **3**, 1311-1318.
27. N. Bizaia, E. H. de Faria, G. P. Ricci, P. S. Calefi, E. J. Nassar, K. A. D. F. Castro, S. Nakagaki, K. J. Ciuffi, R. Trujillano, M. A. Vicente, A. Gil and S. A. Korili, *ACS Appl Mater Interfaces*, 2009, **1**, 2667-2678.
28. C. Li, L. Fu, J. Ouyang, A. Tang and H. Yang, *Appl. Clay Sci.*, 2015, **115**, 212-220.
29. K. Peng, J. Zhang, H. Yang and J. Ouyang, *RSC Adv*, 2015, **5**, 66134-66140.
30. S. Liu and H. Yang, *Energy Technol*, 2015, **3**, 77-83.
31. M. Bagherzadeh, F. Ashouri, L. Hashemi and A. Morsali, *Inorg Chem Commun*, 2014, **44**, 10-14.
32. P. Hu and H. Yang, *Appl. Clay Sci.*, 2010, **48**, 368-374.
33. S. D. Jackson and L. A. Shaw, *Appl Catal A-Gen*, 1996, **134**, 91-99.
34. F. Yılmaz, M. Özer, İ. Kani and Ö. Bekaroğlu, *Catal Lett*, 2009, **130**, 642-647.
35. M. Sabo, A. Henschel, H. Fröde, E. Klemm and S. Kaskel, *J Mater Chem*, 2007, **17**, 3827-3832.
36. A. Henschel, K. Gedrich, R. Kraehnert and S. Kaskel, *Chem Commun*, 2008, 4192-4194.
37. C.-R. Bian, S. Suzuki and K. Asakura, *J Phys Chem B*, 2002, **106**, 8587-8598.
38. S. Hinokuma, H. Fujii, M. Okamoto, K. Ikeue and M. Machida, *Chem Mater*, 2010, **22**, 6183-6190.
39. P. Hu and H. Yang, *Appl. Clay Sci.*, 2013, **74**, 58-65.

40. Y. Turhan, M. Doğan and M. Alkan, *Ind Eng Chem Res*, 2010, **49**, 1503-1513.
41. B. Zhang, Y. Li, X. Pan, X. Jia and X. Wang, *J Phys Chem Solids*, 2007, **68**, 135-142.
42. C. T. Johnston, D. L. Bish, J. Eckert and L. A. Brown, *J Phys Chem B*, 2000, **104**, 8080-8088.
43. R. Takenawa, Y. Komori, S. Hayashi, J. Kawamata and K. Kuroda, *Chem Mater*, 2001, **13**, 3741-3746.
44. D. Varade and K. Haraguchi, *Langmuir*, 2013, **29**, 1977-1984.
45. S. Mukherjee, L. Zhou, A. M. Goodman, N. Large, C. Ayala-Orozco, Y. Zhang, P. Nordlander and N. J. Halas, *J Am Chem Soc*, 2014, **136**, 64-67.

Graphical abstract

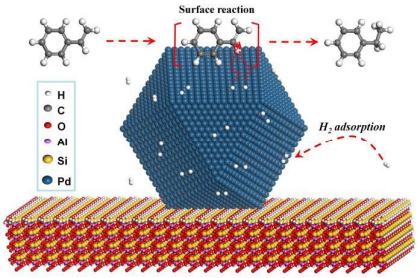

Natural kaolinite nanorod without surface modification served as a mild and outstanding stabilizer for supporting Pd nanoparticles.